

Mechanical properties of gas hydrate-bearing sediments during hydrate dissociation

X. H. Zhang^{1,2} · D. S. Luo¹ · X. B. Lu^{1,2} · L. L. Liu^{3,4} · C. L. Liu^{3,4}

Received: 23 January 2017 / Revised: 7 June 2017 / Accepted: 14 June 2017

© The Chinese Society of Theoretical and Applied Mechanics; Institute of Mechanics, Chinese Academy of Sciences and Springer-Verlag GmbH Germany 2017

Abstract The changes in the mechanical properties of gas hydrate-bearing sediments (GHBS) induced by gas hydrate (GH) dissociation are essential to the evaluation of GH exploration and stratum instabilities. Previous studies present substantial mechanical data and constitutive models for GHBS at a given GH saturation under the non-dissociated condition. In this paper, GHBS was formed by the gas saturated method, GH was dissociated by depressurization until the GH saturation reached different dissociation degrees. The stress–strain curves were measured using triaxial tests at a same pore gas pressure and different confining pressures. The results show that the shear strength decreases progressively by 30%–90% of the initial value with GH dissociation, and the modulus decreases by 50%–75%. Simplified relationships for the modulus, cohesion, and internal friction angle with GH dissociated saturation were presented.

Keywords Gas hydrate-bearing sediments · Dissociation · Mechanical properties · Shear strength · Triaxial test

1 Introduction

From the year 2002 to 2013, the trial productions of gas hydrate (GH) were conducted at the formations of the permafrost-Mallik and Alaska [1,2], and the deep marine-Nankai Trough [3]. The exploitation of GH leads to the GH dissociation from solid to water and gas, and the loss of bearing capacity of gas hydrate-bearing sediments (GHBS). The decrease in the modulus of GHBS increases the compressibility, and dangers of settlement and sliding, especially when the GH stratum is in a slope. The decrease in the shear strength induces the occurrence of soil failures and local stress concentration surrounding the production well [4–6], which is very peculiar in geotechnical engineering.

In nature, GHBS consists of four components, i.e., soil/rock skeleton, GH, water, and gas [7]. Triaxial compression tests were conducted when GH formed in pores of the specimen under a non-dissociation condition, simulating the mechanical behavior before GH exploitation [8–15]. The results indicated that: different GHBS preparation methods such as gas saturated method and water saturated method lead to obvious differences in the mechanical behavior; the GH existence mode in the pores of sediments varies with the increase of GH saturation, leading to the transition of the deformation from shear shrinkage to shear dilatancy. Constitutive models were established to describe the mechanical behaviors of GHBS by using linear elastic or nonlinear elasto-plastic models, such as the Discrete Element Method, Duncan–Chang model, Cam-clay model [16–20]. Those models can consider two or three phases in GHBS, but are incapable of describing the effects of GH dissociation. The knowledge on how the mechanical behaviors change during GH dissociation and the physical mechanism were still insufficient.

✉ X. H. Zhang
zhangxuhui@imech.ac.cn

¹ Institute of Mechanics, Chinese Academy of Sciences, Beijing 100190, China

² College of Engineering, University of Chinese Academy of Sciences, Beijing 100049, China

³ Key Laboratory of Gas Hydrate, Ministry of Land and Resources, Qingdao 266071, China

⁴ Qingdao Institute of Marine Geology, Qingdao 266071, China

A chemo-thermal-mechanically coupled model was established to simulate the soil deformation during GH dissociation, but needs experimental verification [4]. Recent efforts have been made to test the mechanical properties and the softening mechanism of GHBS after complete GH dissociation [21,22]. So then Hyodo et al. [21] conducted tests on the mechanical behaviors under the condition of GH dissociation by the thermal and depressurization method. The shear strength was compared between gas hydrate-bearing Toyoura sand after GH dissociation and pure Toyoura sand. The results indicated that the shear strength of GHBS after thermal induced GH dissociation and isotropic consolidation is less than that of pure Toyoura sand, while no collapse of GHBS occurs after depressurization induced GH dissociation. In addition, Li et al. [22] studied the mechanical behaviors of GHBS containing ice after depressurization and thermal induced GH dissociation. The results showed that the shear strength will decrease after GH dissociation, and the shear strength and modulus under drained conditions are much higher than that under undrained conditions. These studies presented the change of shear strength and modulus after complete GH dissociation by the thermal and depressurization method. However, GH dissociation in GHBS is a progressive process, and the mechanical properties change with the GH dissociation degrees. How the dissociation process affects the mechanical properties is not well understood.

GH dissociation in GHBS brings a new geotechnical problem: (1) the effective porosity and the components varies, and the soil-water characteristic curve depends on the GH dissociation degree; (2) the pore capillary pressure at the pore size of several microns is two orders of magnitude less than both

the pore fluid pressure and confining pressure [7,23]. That is why it is difficult to determine the constitutive relation during GH dissociation.

The aim of this paper is to conduct a series of triaxial tests on silt sandy GHBS considering depressurization induced GH dissociation, obtain the shear strength and modulus at different GH dissociation degrees, and present simplified constitutive models for the shear strength and modulus, describing the progressive soil deformation and failure during the GH exploitation. The paper is organized as follows: In Sect. 2, the specimen preparation and test setups are introduced to illustrate how to obtain the stress–strain relationship of GHBS during GH dissociation. In Sect. 3, the results are compared to show the changes in the mechanical properties at different GH dissociation degrees and effective confining pressures. In Sect. 4, the modulus and shear strength during GH dissociation are analyzed based on the mixed model and Mohr–Coulomb model.

2 GHBS preparation and test setups

Apparatus The tests were conducted on the apparatus of GHBS preparation and triaxial compression (Fig. 1). The apparatus can provide confining pressure ranging from 0 to 14 MPa with an accuracy of 0.5% and temperature from 253.15 to 293.15 K. The maximum back-pressures from 0 to 10 MPa are provided by a gas supply cylinder. A gas flow-meter is used to measure the total gas percolating into the specimen. Then a GHBS specimen with a diameter of 3.9 cm and a height of 8 cm can be formed under proper pressure

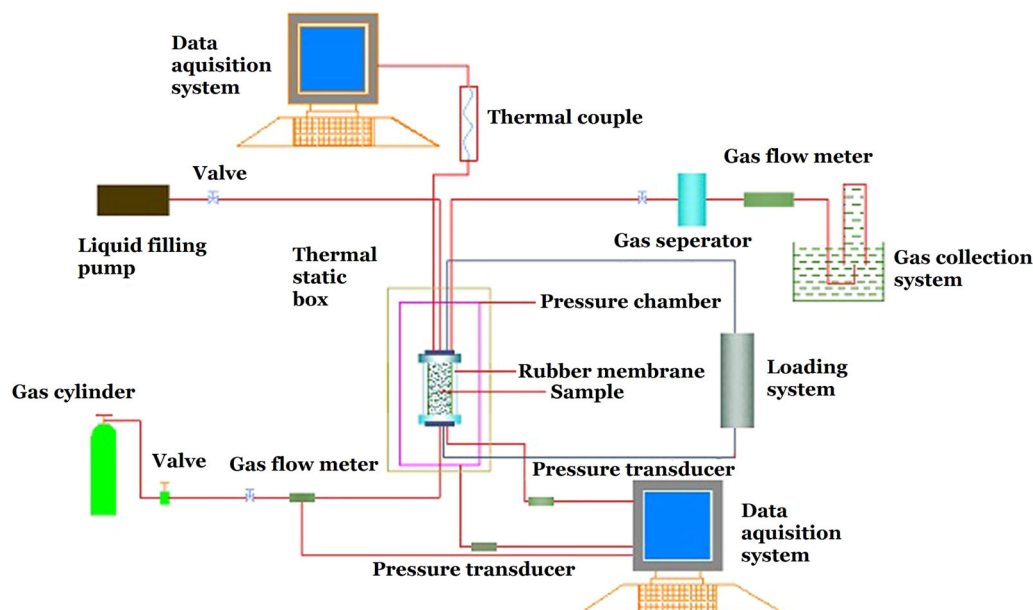


Fig. 1 Test apparatus for GHBS preparation and triaxial compression

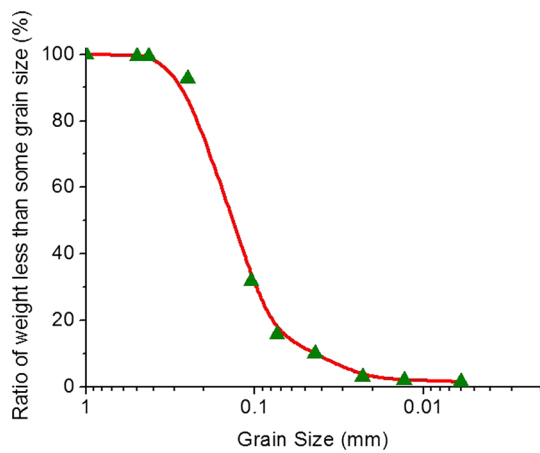


Fig. 2 Grain size distribution of the silt sand

and temperature. The detailed illustration of the apparatus can be referred to Zhang et al. [15].

Soil for preparing specimen Silt sand was used as a skeleton of GHBS whose specific gravity of the sand is 2.69 and the relative density is 54%. The dry density of the specimen is 1.6 g/cm^3 , and the porosity is about 40%. The grain size distribution is shown as in Fig. 2. The radius and height of the specimen are 3.91 and 8 cm, respectively.

Test setups The gas saturated method for GHBS preparation was used [12]. The soil skeleton was prepared first with water content according to the designed initial GH saturation (2–3 mL more water was added considering possible non-reacting water), then methane gas percolated into the specimen, and the total supplied gas volume was controlled by the theoretical value of reacted gas in GH and free gas in the specimen. The water content was controlled as follows: First the water was mixed with the silt sand, and then the soil skeleton was prepared (for GH saturation 19%), or first the soil skeleton was prepared, and then the water was injected into pores of the soil (for GH saturation 38%, 50%). It should be noted that for the case of GH saturation at 19%, the water volume is about 6 mL, and mixing method was appropriate for uniform water distribution in specimens. In the formation of GHBS, the confining pressures were set as 5 MPa, the pore gas pressure was 4 MPa. The temperature was 275.15 K. After the silt sandy GHBS preparation, it is shown that GHBS specimen consisted of three components as soil skeleton, GH, and gas, and GH distributed uniformly along the height of the specimen [24].

The GH dissociation process was achieved as follows: The pressure at the top of the GHBS specimen was lowered to the atmospheric pressure. The free gas flowed out and was collected till the gas pressure equaled the atmospheric pressure, then the GH dissociated slowly, and the released gas was collected for calculating the dissociated GH saturation. The

Table 1 Basic controlling parameters

GH saturation before GH dissociation (%)	GH saturation during GH dissociation (%)
19	10, 0
38	25, 15, 0
50	30, 10, 0

pore pressure reduction spread 13 cm in several seconds in GHBS [24], so a uniform pressure could be reached fast in specimens of the same silt sand skeleton during depressurization. Finally, the pore gas pressure was kept at 4 MPa, and the triaxial compression tests were conducted under different confining pressures of 5, 7, 9 MPa, respectively. The axial load F and axial deformation ΔL were recorded during the tests, then the stress and strain were calculated by F/A and $\Delta L/L$ (here A was the corrected area considering no volume change, and L was the initial height of the specimen). Each compression test lasted for about 13 min, so the GH reformation was nonexistent. After the tests, the GH saturations were back-calculated according to the total released gas from the specimen during tests.

Table 1 presents the basic controlling parameters of the tests, including the GH saturations before dissociation and after partial or complete dissociation. It should be noted that the initial GH saturations were the average values, with errors less than 8%.

The volumetric fraction of each component was measured and calculated after tests. All the water was assumed to form GH in the GHBS preparation. The residual GH volume was obtained by the total GH volume before dissociation minus the dissociated GH volume, and the water volume was calculated by the dissociated GH volume.

It is noted that in all the tests GH was dissociated in silt sandy GHBS by the depressurization method, while final compression tests were completed at the pore gas pressure 4 MPa.

3 Results and discussion

3.1 Experimental results

The stress–strain curves present the behavior of plastic failure, reduction of stiffness and shear strength with GH dissociation which is related with the effective confining pressures and dissociation degrees (Fig. 3). In the following figures CP represents the effective confining pressure. The developing of the curves can be explained as: During GH dissociation, initial continuous linkage of GH is broken, the cementation between GH and skeleton becomes weaker, the gas and water release from the solid GH, and then the

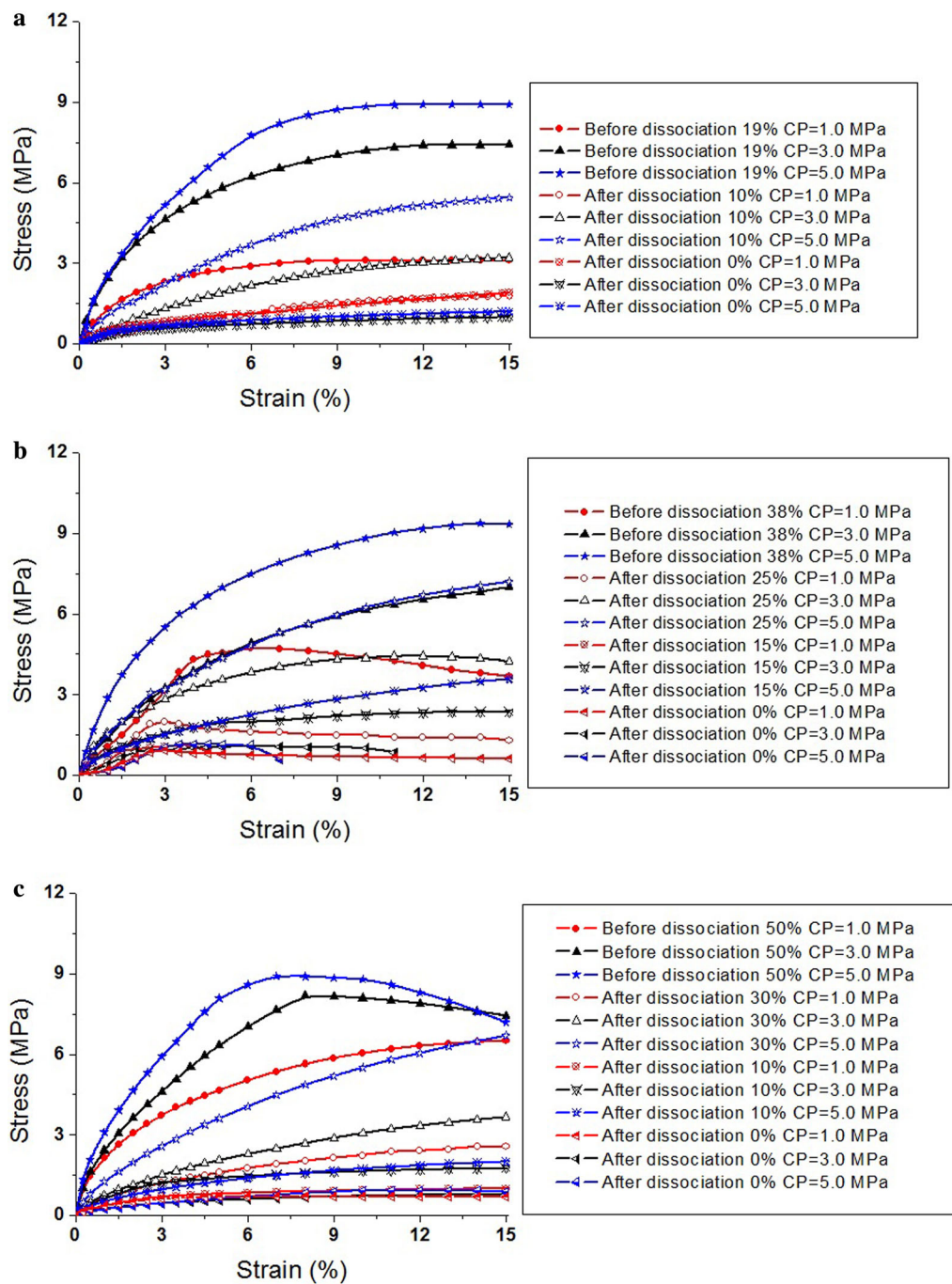


Fig. 3 Stress–strain curves during GH dissociation under different initial GH saturations and effective confining pressures. **a** Initial GH saturation 19%. **b** Initial GH saturation 38%. **c** Initial GH saturation 50%

interface enhancement effects in GHBS is reduced, i.e., the structural properties change greatly.

The shear strength decreases by 35%–83% when the GH dissociates from saturation 19% to 10% and 0%, 50%–90% when GH saturation decreases from 38% to 25%, 15% and 0%, respectively, and 30%–90% when GH saturation decreases from 50% to 30%, 10% and 0%, respectively. In

addition, Winters et al. [9,10] presented similar results that the shear strength of sediments after complete GH dissociation decreases by about 90% of natural GHBS.

Figure 4 presents a comparison among the stress–strain curves at effective confining pressure of 3 MPa when the GH saturation decreases by 90%, 85%, 90% from 50%, 38%, 19%, respectively. The shear strength reduces more for a

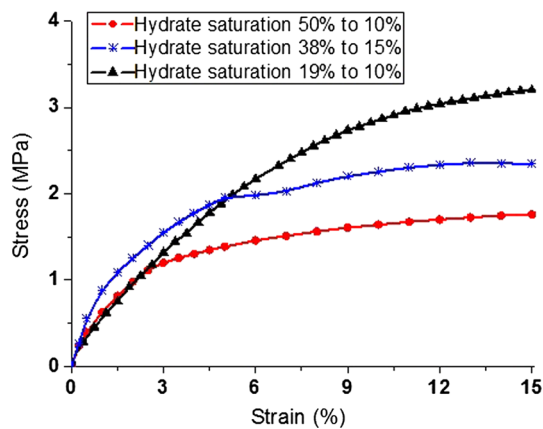


Fig. 4 The stress–strain curves under effective confining pressure of 3 MPa

higher initial GH saturation, while the difference becomes less with the increase of the GH dissociation degree. The phenomenon can be explained that the cementing effect is stronger at a higher initial GH saturation, the GH dissociation first breaks the linkage and cementation among GH and soil grains, more gas and water is released into the pores of GHBS, and then the structural property and shear strength decrease more quickly.

With the increase of GH dissociation, the shear strength decreases in a nonlinear way in Fig. 5. The reason is that during GH dissociation, the components and phase state in GHBS change: the solid component decreases, while the water in the pores increases. Though the gas is released from GH, drainage is applied fast, thus the volumetric fraction of the gas changes only a little. In another point of view, the effective porosity of GHBS increases during GH dissociation, while the shear strength decreases under the same effective stress. The mechanism should be further investigated and revealed from microscopic measurement during the GH dissociation.

The modulus was obtained by computing $\Delta\sigma/\Delta\varepsilon$ at the strain of 0.5%–1% as shown in Fig. 6. The modulus decreases by 50%–75% nonlinearly with GH dissociation. It is to be noted, Li et al. [16] obtained that the modulus decreased by about 50% after depressurization induced GH dissociation in permafrost-associated GHBS under undrained condition. The changes in the components and interfaces of GHBS lead to the variation in the transfer path of force.

3.2 Models for the modulus and shear strength of GHBS during GH dissociation

The variation of components during GH dissociation are described as follows: before GH dissociation, the components consist of soil skeleton, GH, and gas; after partial GH dissociation, soil skeleton, GH, gas, and water; and after com-

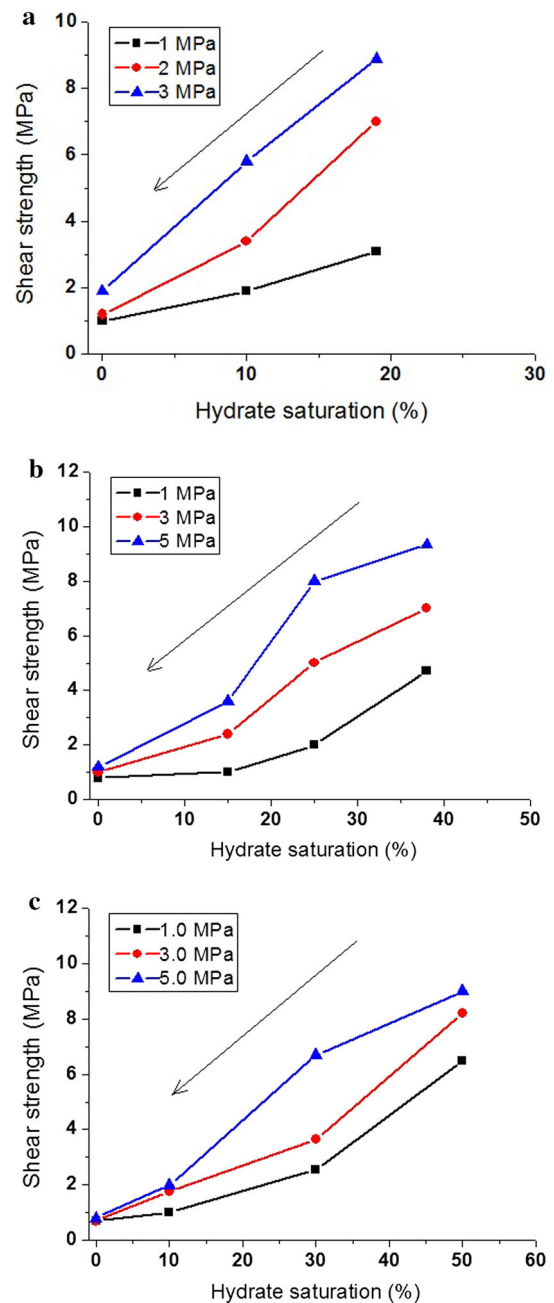


Fig. 5 The change of shear strength under different initial GH saturation. **a** 19% → 10% → 0%. **b** 38% → 25% → 15% → 0%. **c** 50% → 30% → 10% → 0%

plete GH dissociation, soil skeleton, gas, and water. After complete GH dissociation, the water saturations in the pores of the sediments are 0.15, 0.32, 0.40 at initial GH saturation 19%, 38%, 50%, respectively.

3.2.1 The modulus of GHBS during the GH dissociation

The gas is the main component in the pore of GHBS and highly compressible; hence, we consider a two-phase mixed

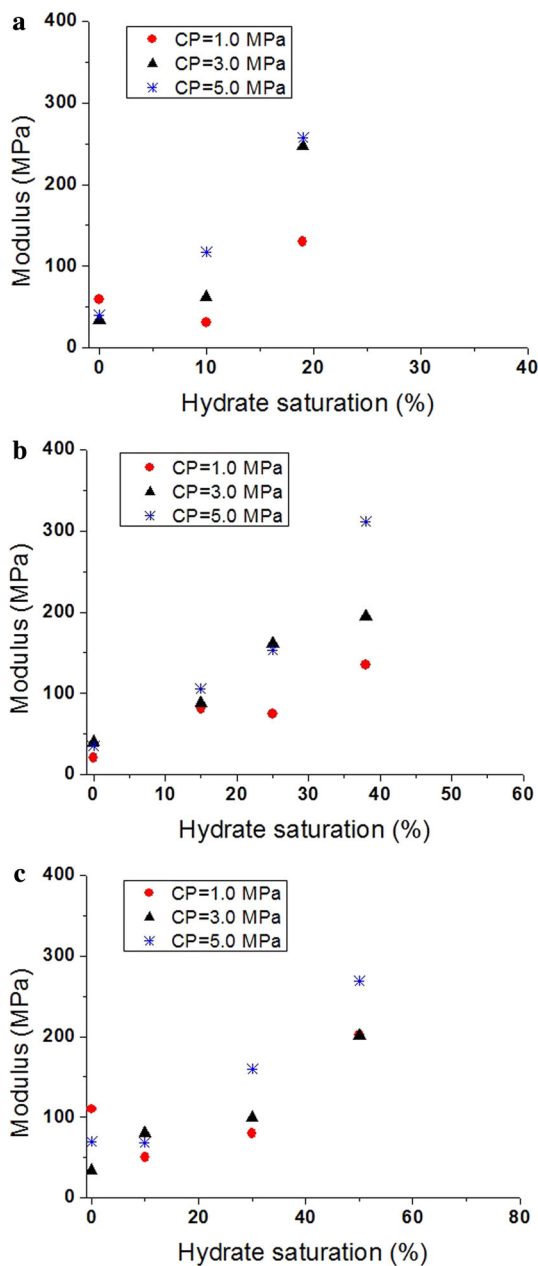


Fig. 6 The change of modulus under different initial GH saturation. **a** 19% → 10% → 0%. **b** 38% → 25% → 15% → 0%. **c** 50% → 30% → 10% → 0%

model to describe the modulus of GHBS during GH dissociation [12]. The gas, water, and soil skeleton (Phase 1: higher compressibility) are regarded as one phase, and GH (Phase 2: lower compressibility) as the other phase. This model is based on the mechanics of compound materials, considering statistical phenomenological characteristics and a series-parallel stress path in GHBS. λ_v and λ_r are introduced to describe the statistical parameters (fractions) of parallel and series modes in GHBS, which satisfy $\lambda_v + \lambda_r = 1$, $\lambda_v \lambda_r \geq 0$.

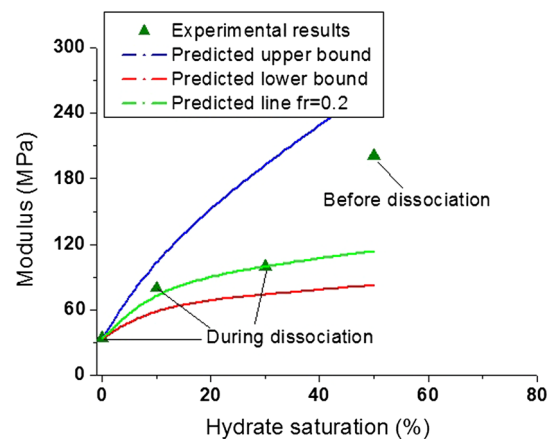


Fig. 7 The modulus of GHBS during the GH dissociation

In Reuss is the low-bound model (the series mode)

$$E_r = \left(\frac{V_1}{E_1} + \frac{V_2}{E_2} \right)^{-1} \tag{1}$$

In Vigot is the upper-bound model (the parallel mode)

$$E_v = E_1 V_1 + E_2 V_2. \tag{2}$$

Assuming GHBS as isotropic material, Zhang et al. [12] present the formulation of the modulus as

$$E = \left[\frac{1}{2} \left(\frac{\lambda_r}{E_r} + \frac{\lambda_v}{E_v} \right) + \frac{1/2}{\lambda_r E_v + \lambda_v E_r} \right]^{-1} \tag{3}$$

The lower and upper bounds of the modulus are

$$E_{\min} = \frac{2E_v E_r}{E_v + E_r}, \quad E_{\max} = \sqrt{E_v E_r}, \tag{4}$$

where E_1 and E_2 represent the modulus of Phase 1 and Phase 2, V_1 and V_2 represent the volumetric fractions of Phase 1 and Phase 2, respectively.

Taken the initial GH saturation of 50% as an example, before GH dissociation, the statistical parameter $\lambda_r=0.5$, and can describe the modulus of GHBS. During GH dissociation, the modulus is close to the predicted lower bound of the mixed model (Fig. 7). The reason is that during GH dissociation, the linkage between GH and soil grains changes, leading to the change in the arrangement mode of the two phases. The stress transfer path and the statistic fractions of series and parallel modes are changed, and the effect of Phase 1 on the modulus prevailed with the increase of GH dissociation.

3.2.2 The shear strength of GHBS during the GH dissociation

According to the Fredlund equation, the shear strength of unsaturated soil can be expressed as

$$\tau_f = c' + (\sigma - P_g) \tan \phi' + (P_g - P_w) \tan \phi'', \quad (5)$$

where, τ_f , σ , P_g , P_w , ϕ' , $c' + (P_g - P_w) \tan \phi''$ represent shear strength, total stress, pore gas pressure, pore water pressure, effective internal friction angle, and effective cohesion, respectively.

Dividing both sides of Eq. (5) by P_g yields

$$\frac{\tau_f}{P_g} = \frac{c'}{P_g} + \frac{P_g - P_w}{P_g} \tan \phi'' + \left(\frac{\sigma}{P_g} - 1 \right) \tan \phi'. \quad (6)$$

At GH saturation of 38%, the pore gas pressure P_g is kept at 4.0 MPa, when the back water pressure P_w is about 3.95 MPa, the water flow is zero. Thus the capillary pressure $P_g - P_w$ is regarded as about 0.05 MPa. From the quantitative analysis, $\frac{P_g - P_w}{P_g}$ was about 10^{-2} . Hence, for the silt sandy GHBS during GH dissociation, the capillary pressure is ignorable compared with the pore fluid pressure, and then the Mohr–Coulomb criterion for gas saturated soil is applied to describe the shear strength. Both the cohesion and internal friction angle decrease with GH dissociation as in Fig. 8.

The dimensionless cohesion and the internal friction angle can be expressed as follows

$$c_{hd}/c_h \sim f_1(S_{hd}/S_h), \quad (7)$$

$$\varphi_{hd}/\varphi_h \sim f_2(S_{hd}/S_h), \quad (8)$$

where c_{hd} , φ_{hd} , S_{hd} represent the cohesion, internal friction angle after partial or complete dissociation, and dissociated GH saturation, respectively. c_h , φ_h , S_h represent the cohesion, internal friction angle, and GH saturation before dissociation, respectively.

The cohesion decreases with GH dissociation degree. The dimensionless cohesion c_{hd}/c_h can be fitted to be a quadratic polynomial of S_{hd}/S_h for the initial GH saturation of 50%, 38%, 19%, respectively

$$c_{hd}/c_h = 1.3 \cdot (S_{hd}/S_h)^2 - 2.2 \cdot (S_{hd}/S_h) + 1.00. \quad (9)$$

The correlation coefficient R^2 is 0.99. The dimensionless cohesion varies with GH dissociation very closely under different initial GH saturations (Fig. 9). The mechanism is interesting and worth further research.

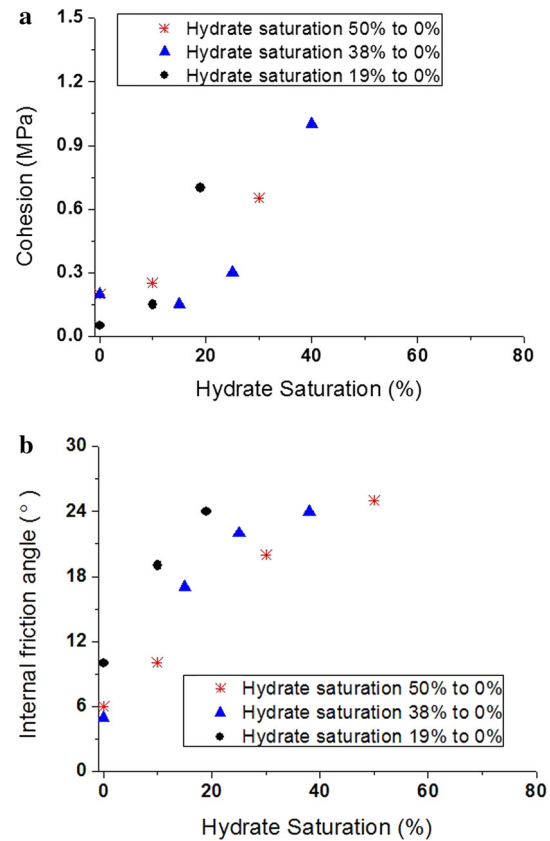


Fig. 8 The cohesion and internal friction angle with the GH dissociation. **a** Cohesion. **b** Internal friction angle

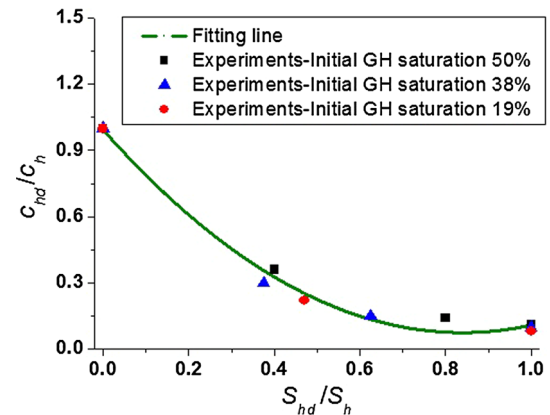


Fig. 9 The cohesion with the GH dissociation

For the initial GH saturation of 50%, 38%, 19%, respectively, the dimensionless internal friction angle φ_{hd}/φ_h can be fitted to be a quadratic polynomial of S_{hd}/S_h

$$\varphi_{hd}/\varphi_h = -0.59 \cdot (S_{hd}/S_h)^2 - 0.16 \cdot (S_{hd}/S_h) + 1.00. \quad (10)$$

The correlation coefficient R^2 is 0.94. The dimensionless internal friction angle varies with GH dissociation in a similar way under different initial GH saturations (Fig. 10).

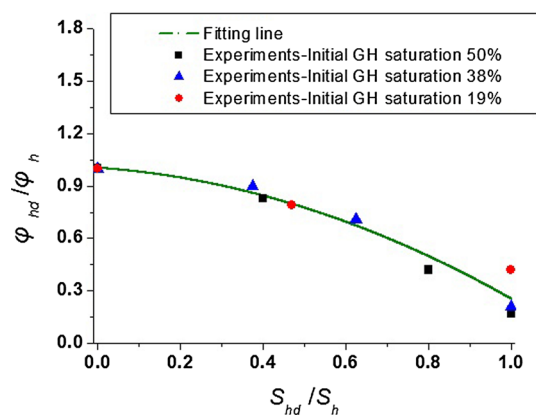


Fig. 10 The internal friction angle with GH dissociation

4 Conclusions

The mechanical properties of silt sandy GHBS during GH dissociation were investigated under different initial GH saturations of 50%, 38%, 19%. A series of tests was conducted in a triaxial apparatus in three stages: first, prepare GHBS by using the gas saturated method; second, dissociate GH by depressurization induced GH dissociation; and third, carry on compression tests at the same pore gas pressure.

The stress–strain relationship presents the behavior of plastic failure. The modulus and shear strength decrease with GH dissociation, and the decreasing percentage is related with the effective confining pressures and dissociation degrees. During the development of GH dissociation, the shear strength decreases by about 30%–90%, and the modulus decreases by about 50%–75%.

Under different initial GH saturations, the shear strengths reduce more for a higher initial GH saturation due to the stronger structural change, breakage of the linkage and cementation between GH and soil grains, and more release of gas and water.

The modulus goes to the lower bound of the mixed model due to the solid GH with a high stiffness turning into the fluid phase with higher compressibility. The cohesion and internal friction angle decrease with the GH dissociation. The relationships between the two dimensionless strength parameters with the relative dissociation degree can be described as quadratic polynomial functions.

GH dissociation changes the volumetric fraction of each component, the pore fluid pressure, and the interaction among the skeleton's grains. The microscopic mechanisms are worth investigating in a further study to reveal the unique phenomenon during GH dissociation.

Acknowledgements The project was supported by the National Natural Science Foundation of China (Grants 41376078, 51639008, and 51239010) the China Geological Survey (Grant DD20160216), and the

Youth Innovation Promotion Association of Chinese Academy of Sciences (Grant 2017027).

References

- Hauge, L. P., Birkedal, K. A., Ersland, G., et al.: Methane production from natural gas hydrates by CO₂ replacement-review of lab experiments and field trial. Society of Petroleum Engineers, SPE-169198-MS (2014)
- Lee, S., Kim, S.: Onshore and offshore gas hydrate production tests. *Econ. Environ. Geol.* **47**, 275–289 (2014)
- Terao, Y., Lay, K., Yamamoto, K.: Design of the surface flow test system for 1st offshore production test of methane hydrate. In: Offshore Technology Conference-Asia, OTC-24719-MS, Malaysia, March 25–28 (2015)
- Kimoto, S., Oka, F., Fushita, T.: A chemo-thermo-mechanically coupled analysis of ground deformation induced by gas hydrate dissociation. *Int. J. Mech. Sci.* **52**, 365–376 (2010)
- Kwon, T.H., Oh, T.M., Choo, Y.W., et al.: Geomechanical and thermal responses of hydrate bearing sediments subjected to thermal simulation: physical modeling using a geotechnical centrifuge. *Energy Fuels* **27**, 4507–4522 (2013)
- Yoneda, J., Masui, A., Konno, Y., et al.: Mechanical properties of hydrate-bearing turbidite reservoir in the first gas production test site of the eastern Nankai trough. *Mar. Pet. Geol.* **66**, 471–486 (2015)
- Waite, W.F., Santamarina, J.C., Cortes, D.D., et al.: Physical properties of hydrate-bearing sediments. *Rev. Geophys.* **47**, 1–38 (2009)
- Clayton, C.R.L., Priest, J.A., Best, A.I.: The effects of disseminated methane hydrate on the dynamic stiffness and damping of a sand. *Geotechnique* **55**, 423–434 (2005)
- Winters, W.J., Pecher, I.A., Waite, W.F., et al.: Physical properties and rock physics models of sediment containing natural and laboratory-formed methane gas hydrate. *Am. Mineral.* **89**, 1221–1227 (2004)
- Winters, W.J., Waite, W.F., Mason, D.H., et al.: Methane gas hydrate effect on sediment acoustic and strength properties. *J. Pet. Sci. Eng.* **56**, 127–135 (2007)
- Miyazaki, K., Masui, A.: Tri-axial compressive properties of artificial methane hydrate bearing sediment. *J. Geophys. Res.* **116**, B06102 (2011)
- Hyodo, M., Li, Y.H., Yoneda, J., et al.: Effects of dissociation on the shear strength and deformation behavior of methane hydrate-bearing sediments. *Mar. Pet. Geol.* **51**, 52–62 (2014)
- Zhang, X.H., Liu, L.L., Zhou, J.B., et al.: A model for the elastic modulus of hydrate-bearing sediments. *Int. J. Offshore Polar* **25**, 314–319 (2015a)
- Zhang, X.H., Lu, X.B., Shi, Y.H., et al.: Study on the mechanical properties of hydrate-bearing silty clay. *Mar. Pet. Geol.* **67**, 72–80 (2015b)
- Zhang, X.H., Lu, X.B., Zhang, L.M., et al.: Experimental study on mechanical properties of methane-hydrate-bearing sediments. *Acta Mech. Sin.* **28**, 1356–1366 (2012)
- Li, Y.H., Song, Y.C., Liu, W., et al.: Analysis of mechanical properties and strength criteria of methane hydrate-bearing sediments. *Int. J. Offshore Polar* **22**, 290–296 (2012)
- Miyazaki, K., Tenma, N., Aoki, K., et al.: A nonlinear elastic model for triaxial compressive properties of artificial methane-hydrate-bearing sediment samples. *Energies* **5**, 4057–4075 (2012)
- Jiang, M.J., Sun, Y.G., Yang, Q.J.: A simple distinct element modeling of the mechanical behavior of methane hydrate-bearing sediments in deep seabed. *Granul. Matter* **15**, 209–220 (2013)
- Pinkert, S., Grozic, J.L.H., Priest, J.A.: Strain-softening model for hydrate-bearing sands. *Int. J. Geomech.* **15**, 04015007 (2015)

20. Pinkert, S., Grozic, J.L.H.: Experimental verification of a prediction model for hydrate-bearing sand. *J. Geophys. Res. Solid Earth* **121**, 4147–4155 (2016)
21. Hyodo, M., Li, Y.H., Yoneda, J., et al.: Mechanical behavior of gas-saturated methane hydrate-bearing sediments. *J. Geophys. Res. Solid Earth* **118**, 5185–5194 (2013)
22. Li, Y.H., Liu, W.G., Zhu, Y.M., et al.: Mechanical behaviors of permafrost-associated methane hydrate-bearing sediments under different mining methods. *Appl. Energy* **162**, 1627–1632(2016)
23. Sha, Z.B., Liang, J.Q., Zhang, G.X., et al.: A seepage gas hydrate system in northern South China sea: seismic and well log interpretations. *Mar. Geol.* **366**, 69–78 (2015)
24. Liu, L.L.: Evolution of gas hydrate dissociation front in hydrate-bearing sediment. [Ph.D. Thesis], Institute of Mechanics, Chinese Academy of Sciences, China (2013)